ELSEVIER

Chemical Geology 193 (2003) 127–136

CHEMICAL GEOLOGY
INCLUDING
ISOTOPE GEOSCIENCE

www.elsevier.com/locate/chemgeo

Phosphor imaging as a tool for in situ mapping of ppm levels of uranium and thorium in rocks and minerals

Jennifer M. Cole[a,*], Jessica Nienstedt[b], Glenn Spataro[b], E. Troy Rasbury[b], Antonio Lanzirotti[c], Aaron J. Celestian[b], Melanie Nilsson[d], Gilbert N. Hanson[b]

[a] *Interdepartmental Doctoral Program in Anthropological Sciences, State University of New York at Stony Brook, Stony Brook, NY 11794-4364, USA*
[b] *Department of Geosciences, State University of New York at Stony Brook, Stony Brook, NY 11794-2100, USA*
[c] *Consortium for Advanced Radiation Sources, University of Chicago, Chicago, IL 60637, USA*
[d] *Oxford Centre for Molecular Sciences, University of Oxford, Oxford OX1 3QH, UK*

Received 14 January 2002; accepted 6 August 2002

Abstract

Phosphor imaging is a type of digital autoradiography that has been widely used in biochemistry to examine radioactively tagged proteins. We used phosphor imaging to map in situ U and Th in polished slabs of geological materials including carbonates, phosphates, and silicate-rich rocks. We examined samples containing between 2 and >500 ppm U and ~ 700 ppm Th to evaluate the applicability of the technique to geological samples. Resolution of 1 mm or better was obtained even for low concentration (~ 10 ppm) samples. These analyses are routine and only require a light box, phosphor screen, and access to a phosphor imager. The technique is nondestructive, relatively inexpensive, and requires very little processing time. We used this technique to identify U- and Th-enriched carbonates and phosphates, and to find "hot spots" of U- and Th-rich minerals in a granodiorite. These high-resolution maps of U and Th allow us to effectively sample for geochronology and identify potentially interesting samples for synchrotron X-radiation studies. The maps produced by phosphor imaging also have great potential for investigating the details of adsorption of radionuclides to rocks and minerals in contaminated areas.

Keywords: Phosphor imaging; Autoradiography; U; Th

1. Introduction

Some techniques used to image U and Th concentrations in situ in geological materials include electron microprobe mapping, fission-track mapping, synchrotron X-ray fluorescence (SXRF) mapping, and film autoradiography. We propose that phosphor imaging is another useful technique to map U and Th. There are three factors that determine a technique's applicability: detection limit, spatial resolution, and ease of use. No one technique is applicable to all types of samples. The phosphor imaging technique outlined

* Corresponding author. Tel: +1-631-632-8294; Fax: +1-631-632-8240.
E-mail address: jenna@pbisotopes.ess.sunysb.edu (J.M. Cole).

0009-2541/02/$ - see front matter © 2002 Elsevier Science B.V. All rights reserved.
PII: S0009-2541(02)00223-1

here is inexpensive, easy to use, and good for moderate spatial resolution. A practical application of phosphor imaging is to help identify areas of rocks and soil samples for further examination with other, higher resolution techniques.

Electron microprobes can be used to map in situ the chemical composition of rocks and minerals (e.g. Spear and Kohn, 1996; McGee and Keil, 2001). The spatial resolution achievable with electron microprobes is high; spot sizes can be as low as 1 μm (Cocherie et al., 1998), depending on concentration. The main limitation of the electron microprobe is relatively low sensitivity compared to other techniques. Although the detection limit for heavy elements such as Th can be as low as 35 ppm (Fialin et al., 1999), minimum concentrations of 150–300 ppm are required for precise measurements of U and Th (Cocherie et al., 1998; Fialin et al., 1999).

Fission-track mapping uses a recorder such as Lexan® plastic to display tracks resulting from the fission of ^{235}U when the sample is irradiated with a neutron flux (Swart, 1988). The fission-track map is a direct representation of U distribution in the sample. The technique has proven useful for looking at U distribution on the tens to hundreds of microns scale in silicate and carbonate rocks (e.g. Zielinski, 1980; Chung and Swart, 1990; Rasbury et al., 2000), and for determining concentrations as low as 10 ppb in carbonate rocks (Swart, 1988). Limits of the use of fission-track mapping are access to a neutron source and the long period of time following neutron bombardment in which the sample is still radioactively hot. Once the sample has been irradiated though, only a petrographic microscope is required to view the results. Fission-track mapping only provides information about U concentrations and variations; the technique cannot detect Th.

Synchrotron X-ray fluorescence (SXRF) analysis is a nondestructive technique that can provide U and Th concentration information (e.g. Hunter and Bertsch, 1998; Phedorin et al., 2000) and has been used to make high-resolution (tens of microns) element maps (Janssens et al., 1994; Bertsch and Hunter, 2001). Usually, the detection limit for U and Th is less than 1 ppm (Bertsch and Hunter, 2001). The intensity of synchrotron radiation permits high-resolution spot sizes, on the order of 5×5 μm, and a fast count rate (Janssens et al., 1993). Others have found SXRF useful for mapping sorbed Pu on geological materials (Duff et al., 2001). A potential complexity of energy dispersive spectral analysis in SXRF is spectral overlap, such as Rb Kα fluorescence on U Lα fluorescence lines. The main limitation of SXRF is that it requires operational expertise and hours of scarce beam time at a synchrotron radiation facility.

Film autoradiography detects strong β- and γ- or α-radiation emitted by radioactive isotopes in samples as recorded on X-ray, photographic, or α-particle-sensitive film (Bowie, 1967; Upham and Englert, 1998). The sample is placed adjacent to film and over time radiation emitted by the sample will cause the film to expose. This type of autoradiography is commonly used on biological materials to detect radioactive tracers introduced to organisms, but has also been applied to geological materials (e.g. Hofmann, 1990; Mironov et al., 1995). Film autoradiography has low detection limits and gives moderate spatial resolution (a few hundreds of microns for enriched samples) (Upham and Englert, 1998). For example, one study of U ore-containing reduction spheroids, containing weight percent U, required 1–3 weeks exposure time for α-particle-sensitive film (Hofmann, 1990). The technique has a high ease of use and only requires darkroom facilities for exposure and developing.

We successfully applied a variety of digital autoradiography called phosphor imaging to study relative U and Th concentrations in geological samples. Phosphor imaging differs from film autoradiography by the use of a storage phosphor screen to record emitted radiation rather than film (Johnston et al., 1990; Upham and Englert, 1998). The storage phosphor screen has higher sensitivity (10–100 times) and reacts more rapidly (at least 10 times) than film (Johnston et al., 1990). Spatial resolution for digitally processed film and phosphor images are roughly equivalent (Upham and Englert, 1998). While SXRF and fission-track mapping have higher resolution and sensitivity, phosphor imaging is complementary as it is relatively inexpensive, nondestructive, and requires little sample preparation. This technique has been used successfully to image radioactive particles from aqueous solutions (Zeissler et al., 2001). Our results show that phosphor imaging is useful for studying the trace elements U and Th in rocks and minerals. This technique is useful for

Fig. 1. We used a Molecular Dynamics™ 445 PhosphorImager®. All pictures are from the Molecular Dynamics website, http://www.mdyn.com (© 2002 Amersham Biosciences. All rights reserved.). (A) Visible-light box "erases" the phosphor screen, causing all of the Eu to convert to the divalent state. (B) Sample is placed on the phosphor screen in a cassette. Radioactivity in the sample will cause the Eu^{2+} to oxidize to Eu^{3+}. (C) Phosphor screen is scanned with a red laser. As the Eu^{3+} returns to the divalent state, photons are emitted and a computer records the resulting image as a digital phosphor image (autoradiograph).

imaging U and Th even for samples with relatively high K contents, probably due to the long half-life and low abundance of ^{40}K even though ^{40}K produces significant γ-rays during decay. Other radioactive elements, such as those that pose a problem for radioactive waste spills, also would be amenable to phosphor imaging. Samples ranging in size from a couple of centimeters to over 20 cm were analyzed,

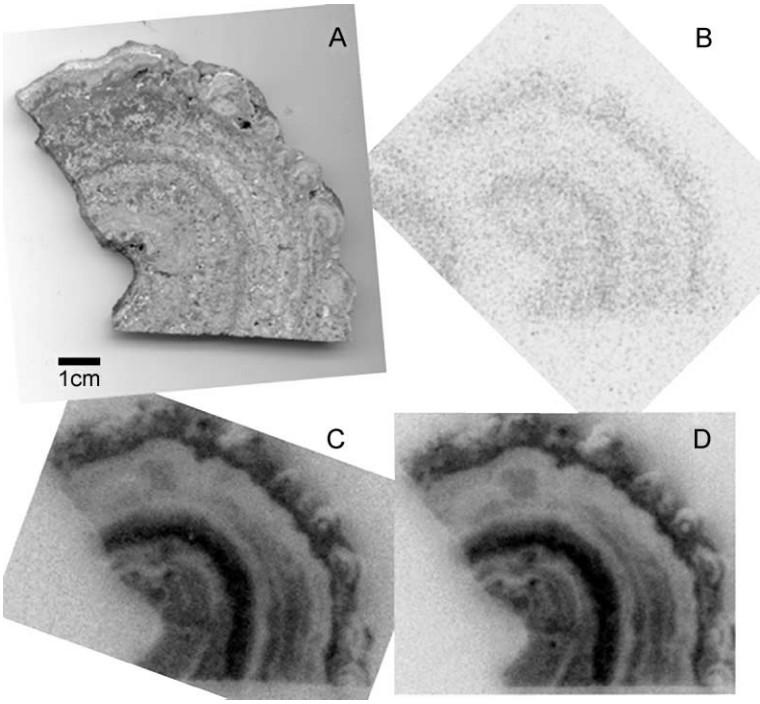

Fig. 2. Miocene tufa calcite sample from the Barstow Formation, Mojave Desert, southern California. (A) Hand specimen. (B) Phosphor image after a 30-min exposure, (C) 4-day exposure, and (D) 1-week exposure. This figure shows that exposure time is dependant on concentration and that there is the potential for overexposure.

demonstrating that this technique is applicable on the hand specimen scale.

2. Materials and methods

2.1. Phosphor imaging

We used a Molecular Dynamics™ 445 PhosphorImager® and a 20 × 25 cm mounted Molecular Dynamics™ storage phosphor screen and cassette for phosphor imaging. Our screens were scanned with the 445 PhosphorImager® housed at the Stony Brook University Microscopy Imaging Center at a cost of about US$10 per scan. Phosphor screens are available for rent from the imaging center at a rate of US$5 per day, but we purchased our own screens through Amersham Biosciences for approximately US$1200 each. Other companies that produce phosphor imagers include Fuji Medical Group USA and Packard Instrument (Defrancesco, 1998). Phosphor imagers sell for between US$20,000 and US$100,000, averaging about US$35,000 (Defrancesco, 1998). Many hospitals and chemistry and biology departments have these types of imagers and may make them available for a nominal charge.

In the storage phosphor technique, a phosphor screen consisting of photostimulable barium fluorobromide (BaFBr) and a trace amount of divalent Eu as a luminescence center is used to detect radiation (Johnston et al., 1990; Upham and Englert, 1998). Energetic β- and γ-radiation emitted from a sample excite the Eu^{2+}, converting it to Eu^{3+}, and releasing an electron (Johnston et al., 1990). This electron is trapped in a bromine vacancy created during the screen manufacturing process (Upham and Englert, 1998). When the phosphor screen is scanned with helium–neon laser at about 633 nm (red light), the trapped electron is released and the Eu^{3+} returns to Eu^{2+}. The Eu reduction emits photons at about 390 nm (blue light) (Johnston et al., 1990; Upham and Englert, 1998). A photomultiplier tube detects the emitted photons and a computer records this energy as a digital image (Upham and Englert, 1998). Variations in intensity on the resulting phosphor image correlate to variations in the concentrations of radionuclides. It should be noted that the phosphor image records radioactivity due to both U and Th. Another technique is required to distinguish between the two elements in samples containing both U and Th.

Fig. 1 illustrates the equipment necessary for phosphor imaging. A visible-light box is used to completely erase the screen of the previous exposure (Fig. 1A). A flatbed scanner also was successfully used for this purpose. Erasing the screen allows it to be reused nearly indefinitely (Johnston et al., 1990). The phosphor screen and the sample are placed in a cassette (Fig. 1B) so that the immobilized sample

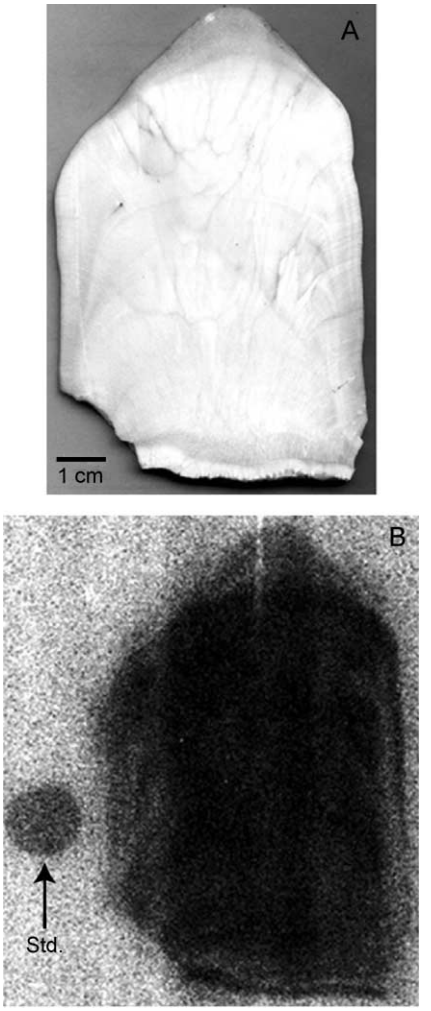

Fig. 3. Aragonite speleothem from Grotte Théophile, Alpe d'Huez, France. (A) Hand specimen. (B) Phosphor image compared to the National Institute of Standards and Technology Standard Reference Material 612. Exposure time was 4 days. This sample shows very homogeneous uranium distribution.

maintains contact with the screen. The exposure time depends on the concentration of radionuclides in the sample. High concentration samples can generate an image in minutes while samples in the low (10–20) ppm range require weeks of exposure. Following exposure, the screen is scanned using a He–Ne laser (Fig. 1C) and a computer generates the resulting digital image.

Natural radiation such as cosmic rays and natural γ-rays contribute significantly to the oxidation of Eu^{2+} in the phosphor screen, and it is not possible to distinguish between this background oxidation and exposure due to radionuclides contained in the sample. Thus, for samples with U and Th in the low ppm range, which will require weeks to generate an image, it is necessary to store the screen in a shielded area, such as a Pb-lined cabinet.

2.2. Sample preparation

Polished slabs of rock up to 20×25 cm were imaged in this study. The optimal sample thickness is less than 1 cm as this allows the cassette containing the phosphor screen to be fully closed, ensuring sample contact with the screen. Since γ-radiation can penetrate quite deep, samples should be cut as thin as possible to make certain the map most closely reflects the details of the polished surface. Polishing the slabs also enables complete, even contact with the plate. Samples, or the phosphor plate itself, are covered in plastic wrap to protect the plate surface. The polished side of the sample is then placed on the plate and exposed for minutes to weeks, depending on U or Th concentration. Phosphor screens were placed in Pb-lined cabinets to reduce background exposure due to cosmic rays and natural γ-radiation during exposure of the samples.

3. Results

We present the results of phosphor imaging on seven geological samples (Figs. 2–8). The first sample is a middle Miocene calcite tufa deposit from the Barstow Formation in southern California (Fig. 2A). This sample has alternating bands of light and darker calcite that are between 0.1 and 1 cm thick. Additionally, there are laminations within the bands on the tens of microns scale. These finer scale laminations are difficult to observe in the hand specimen, but are clear

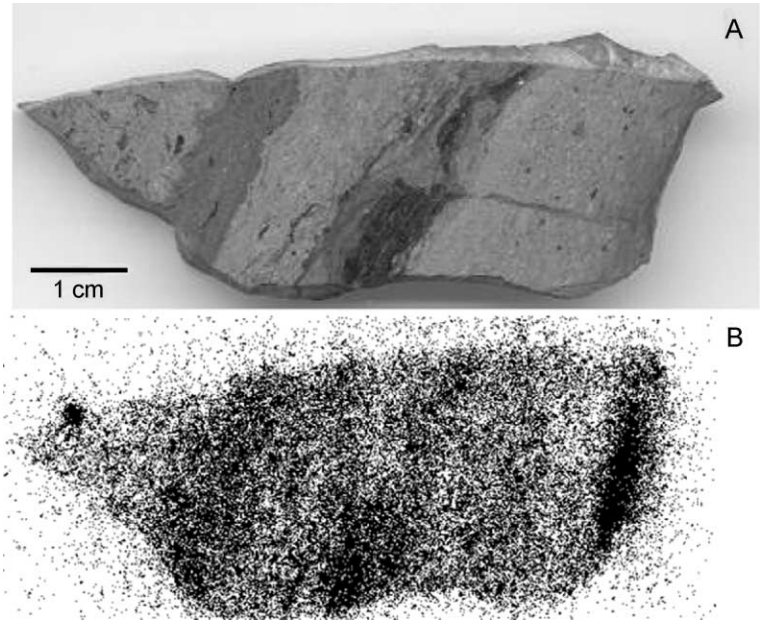

Fig. 4. Late Paleozoic palustrine limestone from the Appalachian Basin, Ohio. (A) Hand specimen. (B) Phosphor image with a 1-week exposure. Phosphor imaging is able to resolve variations in U concentration in this low U sample.

with a magnifying lens and in thin section. Our lab has analyzed this and similar tufa samples for U–Pb dating (Cole et al., 2001) and to study the cyclic nature of U concentrations (Becker et al., 2001). U concentrations range from 68 to 162 ppm as determined by isotope dilution. In situ SXRF analyses show that U concentration exceeds 500 ppm in the most enriched areas of the sample (Cole et al., 2002). U–Pb analyses show very little variation in $^{208}Pb/^{204}Pb$; therefore, Th concentrations in this sample are low. K concentrations are also low in calcite. This sample was exposed to the phosphor screen for varying amounts of time to determine the optimal exposure time (Fig. 2B–D). Banding in the phosphor image shows variations in U concentration that can be compared to macroscopic variations in the hand specimen, but the finer laminations are only detectable with fission track maps and with high resolution SXRF line scans. As exposure time increases, the intensity of the image also increases. However, increased exposure time also leads to increased background radiation exposure. This background exposure was observed even though our screens were shielded in Pb-lined cabinets.

An aragonite speleothem from Grotte Théophile, Alpe d'Huez, France is shown in Fig. 3A. The sample has 72 ppm U as determined by U–Th alpha spectrometry (Audra and Quinif, 1997). As expected from the homogenous appearance of the hand specimen, this sample shows roughly even U distribution (Fig. 3B). The thinner areas of the hand specimen appear lighter in the phosphor image. Next to the sample is a National Institute of Standards and Technology 3 mm trace element in glass standard (SRM 612). The certificate values for U and Th are 37.38 and 37.79 ppm, respectively. There is also approximately 64 ppm K in the standard. The phosphor image of the sample is more intense than the standard because the sample is thicker, contains more U than the standard, and contains the U-series intermediate daughter products while the standard is enriched only in the parents (Fig. 3B).

In order to understand the lower concentration limits of phosphor imaging, a sample of palustrine limestone from the Late Paleozoic Appalachian Basin, Ohio (Fig. 4) and a sample of paleosol caliche on host dolomite from the Late Paleozoic Permian Basin, western Texas (Fig. 5) were analyzed. The palustrine sample has between 13 and 33 ppm U as determined by isotope dilution (Becker et al., 2000). The paleosol calcite has between 4 and 8 ppm U based on isotope dilution (Rasbury et al., 1997) and 2–20 ppm based on SXRF (McCall et al., 2002). Both samples have

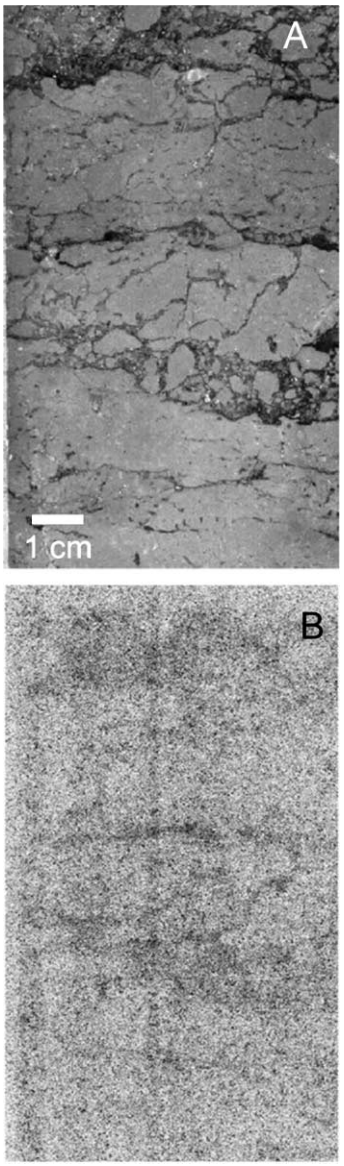

Fig. 5. Late Paleozoic carbonate host with paleosol calcite from the Permian Basin, western Texas. (A) Hand specimen. (B) Phosphor image. Sample was exposed for 4 weeks. Uranium concentrations are low but variable in this sample.

areas of darker brown, organic-rich calcite related to the pedogenesis and lighter brown, organic-poor calcite of the host carbonate (Figs. 4A and 5A). The palustrine limestone was exposed for 1 week and the paleosol limestone for 4 weeks. The phosphor imaging results from both samples show phosphor imaging is capable of resolving variations in U concentrations in the 5–30 ppm range (Figs. 4B and 5B).

Another tufa deposit (phytoherm) from the middle Miocene Barstow Formation was analyzed to examine the U distribution in a variety of mineral phases. This sample (Fig. 6A) has a micritic calcite framework that was filled in first with calcite spar and finally with chalcedony. Isotope dilution analyses of the micrite show a range in U concentrations between 17 and 31 ppm. In the autoradiograph, high U concentrations seem to be limited to the micritic calcite, and it appears that the darker micrite is usually particularly enriched (Fig. 6B). Surprisingly, the chalcedony does seem to concentrate U even though other studies show an affinity of U for cryptocrystalline silica (e.g., Neymark et al., 2000). This sample illustrates the potential to see inter- and intra-mineralogical differences in U concentrations.

A fossilized fish from the Eocene Green River Formation (Fig. 7A) was selected to analyze a Th-rich mineral with phosphor imaging. The fish fossil was determined by in situ X-ray powder diffraction analyses to be composed of fluorapatite (francolite). A 19-h exposure time yielded a spectacular image showing high levels of radionuclides in the fossil (Fig. 7B). The lacustrine host rock also contained moderate levels of U or Th. SXRF analyses show that the fossil has high levels of Th, between 680 and 750 ppm, (Fig. 7C) and low concentrations of U.

Our final sample shows that phosphor imaging can be used to find "hot spots" of U- or Th-rich minerals, such as zircon or monazite, in a K-bearing rock. Fig. 8A shows a slab of a granodiorite boulder found on Long Island. The sample was stained to show K-feldspar and Na-feldspar (Waldemar Pacholik, personal communication, 2001). The larger grain size of the K-feldspar suggests that mineral crystallized early in the cooling history of the granodiorite. The sample was exposed for 4 days (Fig. 8B) and for 3 weeks (Fig. 8C). Hot spots of U- or Th-rich minerals stand out well in the 4-day exposure image. The areas of the granodiorite composed of K-feldspar are the lightest

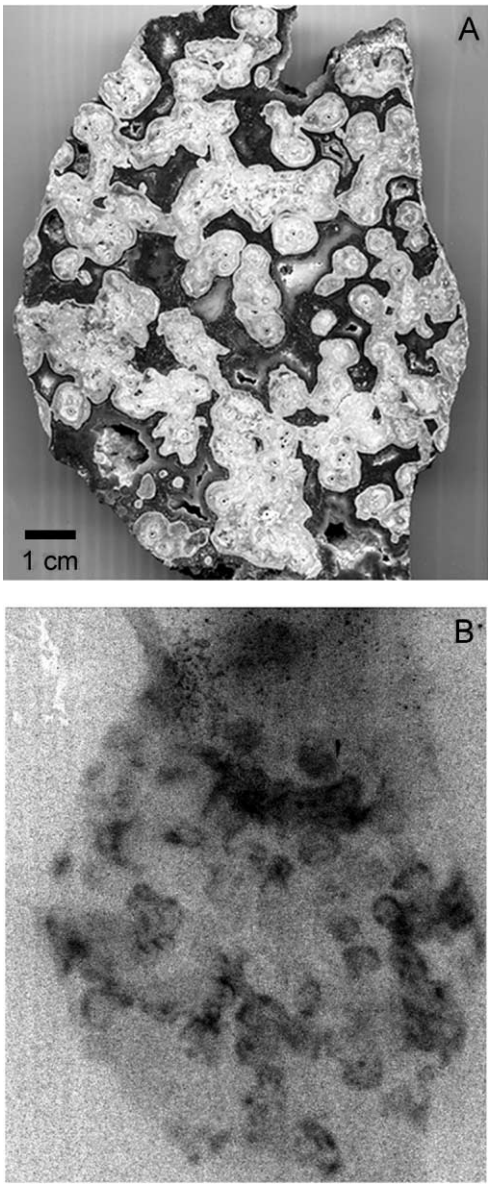

Fig. 6. Miocene tufa deposit composed of micritic calcite, sparry calcite, and chalcedony. Sample is from the Barstow Formation, southern California. (A) Hand specimen. (B) Phosphor image with a 1-week exposure. Uranium concentration is quite variable in the micritic calcite and is much lower in the chalcedony.

in the phosphor image. The intergranular material is seen as more enriched in U. K does not seem to contribute to the exposed image even though ^{40}K is radioactive. This is because the intensity of γ-radia-

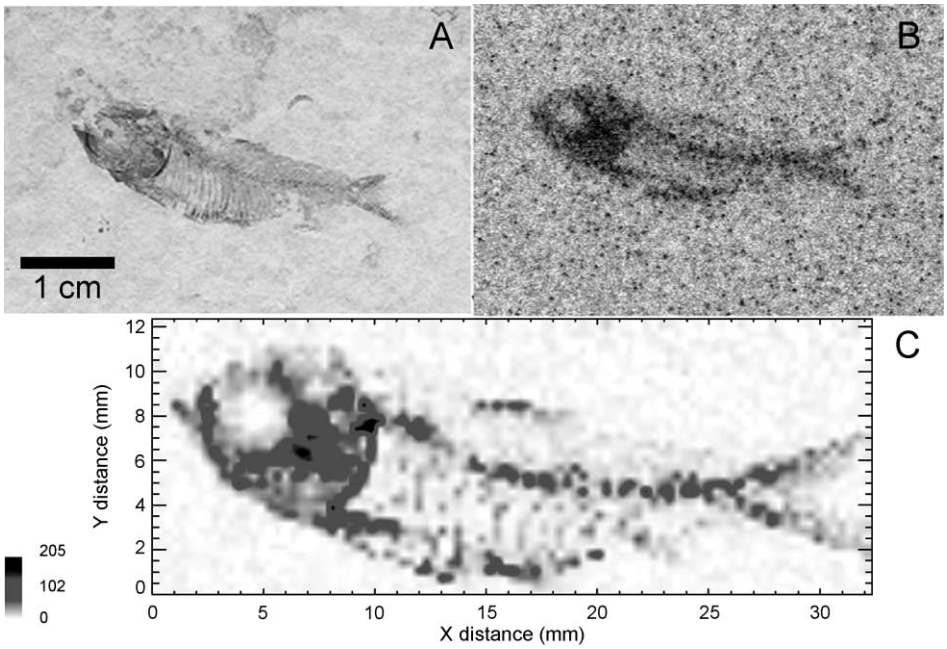

Fig. 7. Fossilized fish from the Eocene Green River Formation, Wyoming. (A) Hand specimen. (B) Autoradiograph resulting from a 19-h exposure. (C) Energy dispersive synchrotron X-ray florescence map of Th $L\alpha_1$ fluorescence counts (normalized to incident beam flux). Darker colors indicate more counts; however, the density of counts within the fish is correlated to the thickness of the fossil and probably does not reflect variable incorporation of Th in the fluorapatite. Data were collected in situ, at atmosphere, with a monochromatic X-ray beam tuned to ~ 17.2 keV at beamline X26A at the National Synchrotron Light Source.

tion emitted by ^{40}K is small relative to that emitted by ^{232}Th, ^{235}U, ^{238}U, and their respective intermediate daughter products. In these phosphor images (Fig. 8B and C), the effect of sample thickness is especially apparent. Along the side of the sample, exposure beyond the limits of the sample is discernable. Gamma-radiation in the sample will travel in any direction, so the fuzziness along the sides of the sample represents γ-rays that traveled from the sample at an oblique angle and subsequently exposed the plate. Decreasing sample thickness minimizes this effect.

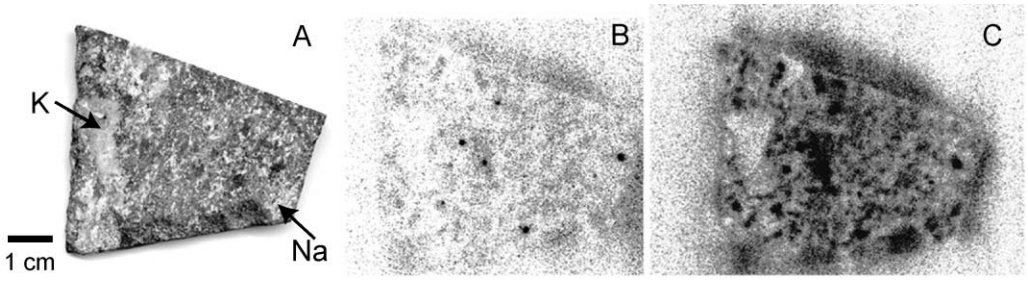

Fig. 8. Slab from a granodiorite boulder found on Long Island. (A) Hand specimen. Granite was stained to show K-feldspar and Na-feldspar. Autoradiography images resulting from a (B) 4-day and a (C) 3-week exposure time. Hot spots of U- or Th-rich minerals can be clearly seen in this sample despite the presence of K-rich minerals.

4. Discussion

Phosphor imaging is a useful tool for in situ determination of relative U and Th concentrations in geological samples such as carbonates, phosphates, and silicates. Phosphor imaging has relatively low detection limits (~ 5–10 ppm), moderate spatial resolution (≤ 1 mm), and a high ease of use. The radioactive isotope of K does not provide enough γ-radiation to expose the phosphor plate, so this tool is useful for mapping U and Th in K-feldspar-bearing rocks. This technique is especially applicable to samples on the hand specimen scale. One potential use of this technique is to aid in sampling of U- and Th-enriched rocks and minerals for U–Pb, Th–Pb, and U-series dating. Another application is to select samples for higher resolution studies of actinides with an electron microprobe or with synchrotron X-radiation.

Acknowledgements

We would like to thank Greg Rudoman of the University Microscopy Imaging Center, State University of New York at Stony Brook, for technical support and assistance. Philippe Audra, Mona Becker, Isabel Montañez, Waldemar Pacholik, Vicki Pedone, and Ann Rasbury provided samples. Beamline personnel at X26A at the National Synchrotron Light Source are thanked for their assistance. An NSF grant (EAR 9814639) and a Stony Brook University–Brookhaven National Lab Seed Grant to Troy Rasbury, and a Department of Energy grant (DER-GO294ER14449) to Gilbert Hanson and William Meyers provided funding. Research was carried out in part at the NSLS, Brookhaven National Laboratory, which is supported by the Department of Energy, Division of Materials Sciences and Division of Chemical Sciences. We thank Eric Oelkers for editorial handling and an anonymous reviewer. **[EO]**

References

Audra, P., Quinif, Y., 1997. Une cavité de haute-montagne originale: La grotte Théophile (Alpe d'Huez, France)—Rôle des paléoclimats Pléistocène dans la spéléogenèse. Spéléochronos 8, 23–32.

Becker, M.L., Rasbury, E.T., Hanson, G.N., Nadon, G.C., Gierlowski-Kordesch, E.H., Kallini, K.D., 2000. U–Pb ages of paleosol and lake calcite from the Appalachian Basin, southeastern Ohio and western Pennsylvania. Abstr. Programs - Geol. Soc. Am. 32 (7), A389.

Becker, M.L., Cole, J.M., Rasbury, E.T., Pedone, V.A., Montañez, I.P., Hanson, G.N., 2001. Cyclic variations of uranium concentrations and oxygen isotopes in tufa from the middle Miocene Barstow Formation, Mojave Desert, California. Geology 29 (2), 139–142.

Bertsch, P.M., Hunter, D.B., 2001. Applications of synchrotron-based X-ray microprobes. Chem. Rev. 101 (6), 1809–1842.

Bowie, S.H.U., 1967. Autoradiography. In: Zussman, J. (Ed.), Physical Methods in Determinative Mineralogy. Academic Press, New York, pp. 467–473.

Chung, G.S., Swart, P.K., 1990. The concentration of uranium in freshwater vadose and phreatic cements in a Holocene ooid cay: a method of identifying ancient water tables. J. Sediment. Petrol. 60 (5), 735–746.

Cocherie, A., Legendre, O., Peucat, J.J., Kouamelan, A.N., 1998. Geochronology of polygenetic monazites constrained by in situ electron microprobe Th–U–total lead determination: implications for lead behaviour in monazite. Geochim. Cosmochim. Acta 62 (14), 2475–2497.

Cole, J.M., Rasbury, E.T., Montañez, I.P., Pedone, V.A., Hemming, S.R., Lanzirotti, A., Becker, M.L., Hanson, G.N., 2001. Uranium–lead ages of lake margin tufa calcite from the middle Miocene Barstow Formation, southern California. Eos Trans. AGU, Fall Meet. Suppl. 82 (47), V42F-04.

Cole, J.M., Lanzirotti, A., Rasbury, E.T., Hanson, G.N., 2002. XRF and XANES studies of uranium incorporation into Miocene tufa calcite. National Synchrotron Light Source Activity Report, Abstract Cole117.

Defrancesco, L., 1998. Illuminating images: the world of phosphor screen and fluorescence imaging systems. Scientist 12 (4), 16.

Duff, M.C., Hunter, D.B., Triay, I.R., Bertsch, P.M., Kitten, J., Vaniman, D.T., 2001. Comparison of two micro-analytical methods for detecting the spatial distribution of sorbed Pu on geological materials. J. Contam. Hydrol. 47 (2–4), 211–218.

Fialin, M., Rémy, H., Richard, C., Wagner, C., 1999. Trace element analysis with the electron microprobe: new data and perspectives. Am. Mineral. 84 (1–2), 70–77.

Hofmann, B.A., 1990. Reduction spheroids from northern Switzerland: mineralogy, geochemistry and genetic models. Chem. Geol. 81 (1–2), 55–81.

Hunter, D.B., Bertsch, P.M., 1998. In situ examination of uranium contaminated soil particles by micro-X-ray absorption and micro-fluorescence spectroscopies. J. Radioanal. Nucl. Chem. 234 (1–2), 237–242.

Janssens, K., Vincze, L., Adams, F., Jones, K.W., 1993. Synchrotron radiation-induced X-ray microanalysis. Anal. Chim. Acta 283 (1), 98–119.

Janssens, K., Vincze, L., Rubio, J., Adams, F., Bernasconi, G., 1994. Microscopic X-ray fluorescence analysis invited lecture. J. Anal. At. Spectrom. 9 (3), 151–157.

Johnston, R.F., Pickett, S.C., Barker, D.L., 1990. Autoradiography using storage phosphor technology. Electrophoresis 11 (5), 355–360.

McCall, K., Lanzirotti, A., Rasbury, E.T., 2002. Uranium (IV) incorporation in paleosol calcite: evidence for sequestration of U on geologic time scales. National Synchrotron Light Source Activity Report 2001, Science Highlights: 2-93–2-96.

McGee, J.J., Keil, K., 2001. Application of electron probe microanalysis to the study of geological and planetary materials. Microsc. Microanal. 7 (2), 200–210.

Mironov, A.G., Zhmodic, S.M., Ochirov, Y.C., 1995. Determination of gold and uranium mineralization in black schists and sulfide ores using radiography complex. Radiat. Meas. 25 (1–4), 495–498.

Neymark, L.A., Amelin, Y.V., Paces, J.B., 2000. $^{206}Pb-^{230}Th-^{234}U-^{238}U$ and $^{207}Pb-^{235}U$ geochronology of Quaternary opal, Yucca Mountain, Nevada. Geochim. Cosmochim. Acta 64 (17), 2913–2928.

Phedorin, M.A., Goldberg, E.L., Bobrov, V.A., Khlystov, O.M., Grachev, M.A., 2000. Multi-wavelength synchrotron radiation XRF determination of U and Th in sedimentary cores from Lake Baikal. Geostand. Newsl. 24 (2), 217–226.

Rasbury, E.T., Hanson, G.N., Meyers, W.J., Saller, A.H., 1997. Dating the time of sedimentation using U-Pb ages for paleosol calcite. Geochim. Cosmochim. Acta 61 (7), 1525–1529.

Rasbury, E.T., Meyers, W.J., Hanson, G.N., Goldstein, R.H., Saller, A.H., 2000. Relationship of uranium to petrography of caliche paleosols with application to precisely dating the time of sedimentation. J. Sediment. Res. 70 (3), 604–618.

Spear, F.S., Kohn, M.J., 1996. Trace element zoning in garnet as a monitor of crustal melting. Geology 24 (12), 1099–1102.

Swart, P.K., 1988. The elucidation of dolomitization events using nuclear-track mapping. In: Shukla, V., Baker, P.A. (Eds.), Sedimentology and Geochemistry of Dolostones. SEPM Special Publication, vol. 43, pp. 11–23.

Upham, L.V., Englert, D.F., 1998. Radionuclide imaging. In: L'Annunziata, M.F. (Ed.), Handbook of Radioactivity Analysis. Academic Press, New York, pp. 647–692.

Zeissler, C.J., Lindstrom, R.M., McKinley, J.P., 2001. Radioactive particle analysis by digital autoradiography. J. Radioanal. Nucl. Chem. 248 (2), 407–412.

Zielinski, R.A., 1980. Uranium in secondary silica: a possible exploration guide. Econ. Geol. 75 (4), 592–602.